# Chapter 22

# ATMOSPHERIC EMISSION AND ABSORPTION OF ULTRAVIOLET RADIATION

R. E. Huffman

## 22.1 VUV/UV BACKGROUND ATMOSPHERIC RADIANCE

The radiance of the earth's atmosphere as seen from space is shown in Figure 22-1. The day and night radiance levels are shown for the earth-center or nadir viewing direction with the observer at an altitude of about 500 km or more. The units are Rayleigh per Å with a Rayleigh equal to $10^6$ photon/(s $cm^2$ column 4 $\pi$ steradian). The values in Figure 22-1 are based on a number of rocket and satellite observations. Only prominent spectral features are shown.

The day radiance values are shown in the upper part of Figure 22-1. The upper curve labeled day maximum gives observed radiance values for overhead sun (solar zenith angle of zero). The radiance is less for larger solar zenith angles. At wavelengths longer than about 2000 Å in the figure, solar scatter is the principal component. Representative references are Elliot et al. [1967], Barth and Mackey [1969], Huffman et al. [1980], and Rawcliffe and Elliot [1966]. Two broad minima are present, centered at about 2500 Å due to ozone and at about 1500 Å due to oxygen. In each case, the atmospheric constituent absorbs back-

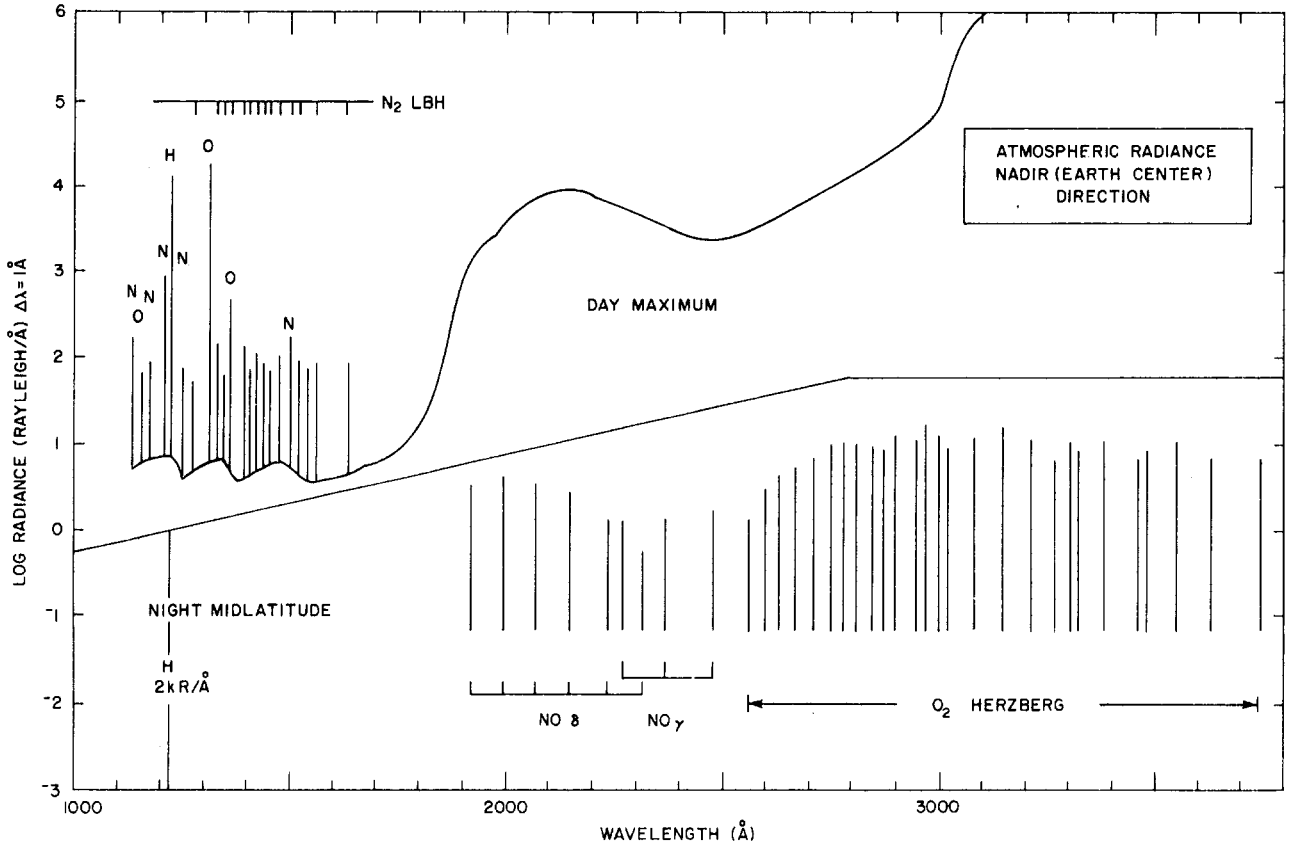


Figure 22-1. Atmospheric radiance in the ultraviolet.

scattered emission leading to a minimum in the background [Heath, 1973].

The emission at wavelengths shorter than 2000 Å in the figure is due primarily to the dayglow. The Lyman-Birge-Hopfield (LBH) bands of molecular nitrogen are the most prominent band system [Meier et al., 1980; Huffman et al., 1980; Prinz and Meier, 1971; Takacs and Feldman, 1977]. Strong multiplets of atomic oxygen occur at 1304 and 1356 Å, and there are several lines of atomic nitrogen, with the strongest at 1493 and 1200 Å. Hydrogen Lyman-alpha (1216Å) emission due to solar resonance scattering from the geocorona has been extensively measured for both day and night situations [Carruthers et al., 1976; Meier and Mange, 1970, 1973; Thomas, 1963].

The night midlatitude radiance values in the lower part of Figure 22-1 are representative of observations found between the tropical ultraviolet airglow belts and the auroral region. The nitric oxide delta and gamma bands and the oxygen Herzberg band emission are due to chemiluminescence. References to these bands are as follows: Cohen-Sabban and Vuillemin [1973]; Huffman et al. [1980]; and Reed and Chandra [1975]. The minimum value in a band centered at 1550 Å was measured by Huffman et al. [1980].

There are several localized sources of ultraviolet emission from the atmosphere, as summarized in Table 22-1. The tropical ultraviolet airglow, due to radiative recombination of oxygen ions, occurs mainly in the pre-midnight sector [Barth and Schaffner, 1970; Carruthers and Page, 1976; and Hicks and Chubb, 1970]. The twilight spectrum is seen near the terminator when only upper altitudes are illuminated by solar ultraviolet, resulting in a low background from solar scatter [Gerard et al., 1970; Barth et al., 1973]. The auroral region as seen from space in the ultraviolet produces many emission features, as measured by Beiting and Feldman [1978]; Chubb and Hicks [1970]; Peek [1970]; and Huffman et al. [1980].

The extreme ultraviolet wavelength region from about 1100 Å to the soft x-ray region near 100 Å has not been as well characterized as VUV/UV wavelengths. Emission is primarily oxygen and nitrogen lines. Rocket observations available to date are by Christensen [1976], Gentieu et al. [1979], and Feldman et al. [1981].

## 22.2 ABSORPTION AND IONIZATION CROSS SECTIONS OF MAJOR GASES

A general introduction to the role of ultraviolet absorption and ionization in aeronomy is given by Watanabe [1958], although most of the cross-section values have been obtained at improved resolution in later work. The major gases discussed here are $O_2$, $O_3$, $N_2$, and O. Cross sections for use in aeronomy are available from several sources: Huffman [1969]; Hudson [1971]; Kirby et al. [1979]. These compilations generally concentrate on solar emission features.

A detailed review including the major atmospheric gases is available by Berkowitz [1979]. Complete bibliographies of photon cross-section references can be obtained through the Low Energy Atomic Collision Cross-Section Information Center, Joint Institute for Laboratory Astrophysics, University of Colorado, Boulder, Colorado 80309.

The transmission through a gas is given by $\exp[-\sigma N]$, where $\sigma$ is the total absorption cross section in $cm^2$ and N is the column density in $cm^{-2}$. The photoionization cross section is the portion of $\sigma$ that results in ionized products. Specific cross sections for producing specific ionized or neutral products can be defined in a similar manner. The cross section must be measured at a resolution considerably less than any structure in the spectrum. This difficulty occurs for narrow lines, and in these regions the simple exponential transmission calculation is not accurate.

Cross sections are given in Figure 22-2 for molecular oxygen ($O_2$) and ozone ($O_3$) and in Figure 22-3 for molecular nitrogen ($N_2$) and atomic oxygen (O). These figures give the location in wavelength of the photon absorption of most importance to aeronomic problems. In regions of complicated structure such as molecular bands or atomic lines, representative values are shown. In these regions, the detailed measurements must be utilized, as found through the

Table 22-1. Ultraviolet emission from localized sources

| Source | Constituent | Nadir Intensity | Remarks |
|---|---|---|---|
| Aurora | O,N Lines<br>$N_2$ Bands<br>(NO?) | up to 10 kR<br>(variable) | Arcs and diffuse aurora seen day and night in auroral oval. |
| Tropical UV Airglow | O 1304,1356 | up to 1 kR<br>(variable) | Night, two bands ± 10° from dip equator. |
| Twilight | NO (Gamma bands)<br>$Mg^+$ | up to 1 kR<br>up to 100R | Near terminator only |

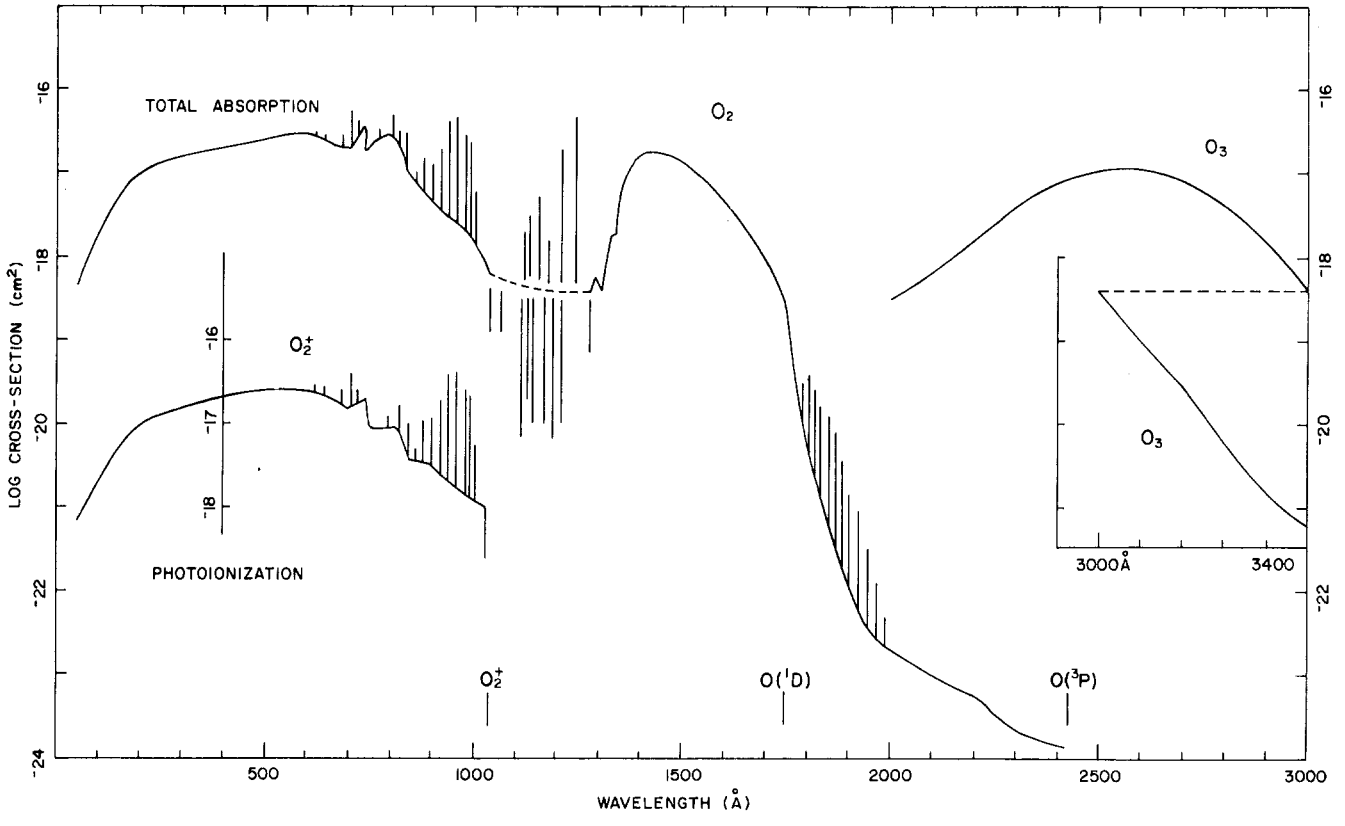


Figure 22-2. Molecular oxygen ($O_2$) and ozone ($O_3$) photon cross sections. Detailed structure and all molecular bands are not shown. See text for further discussion.

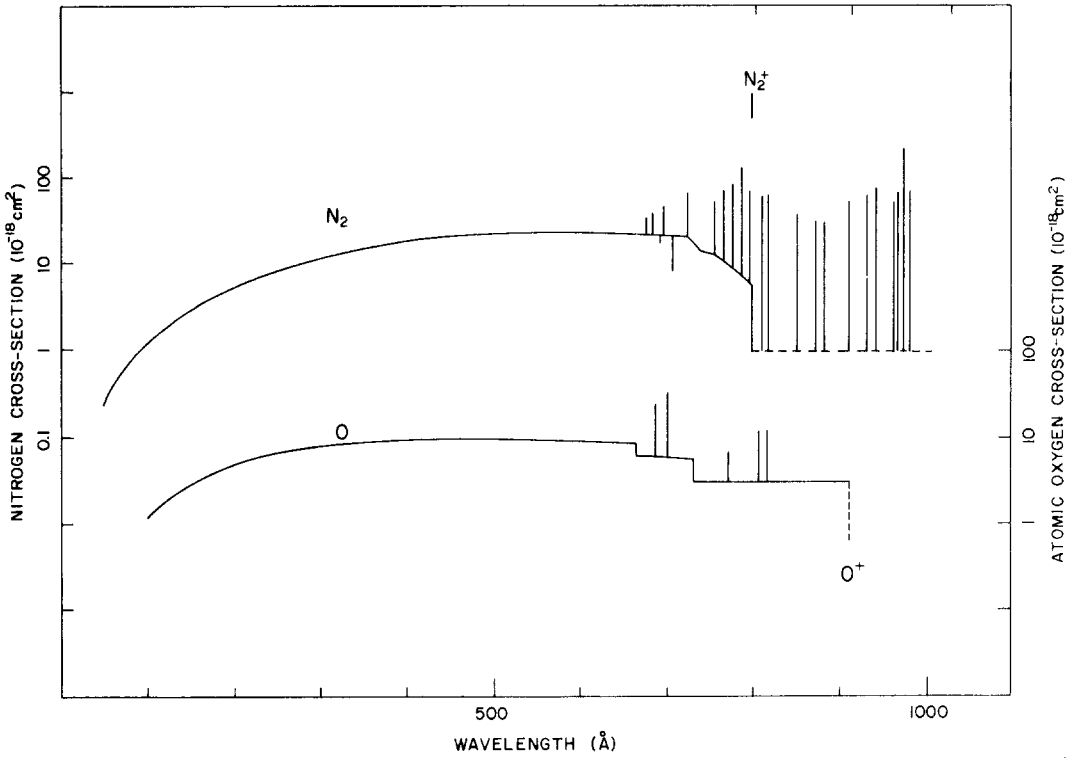


Figure 22-3. Molecular nitrogen ($N_2$) and atomic oxygen (O) photon cross sections. Detailed structure and all molecular bands and atomic lines are not shown. See text for further discussion.

references. The curves given are based on measurements from many sources. Reference to measurements will be necessary for detailed cross sections, especially where discrete structure is indicated.

Molecular oxygen ($O_2$) absorption occurs weakly in the Herzberg continuum between about 2400 and 2050 Å. The Schumann-Runge bands are located between about 1750 and 2050 Å. These bands are composed of many narrow rotational lines. Transmission models have been developed [Blake, 1979]. The Schumann-Runge continuum occurs between about 1250 and 1750 Å. The region between 1027 and 1250 Å has a number of "windows," or regions of low absorption, as well as strong absorption bands. Nitric oxide is photoionized by the intense solar hydrogen Lyman-alpha line (1216 Å) at one of these windows with an ionization cross section of $2.0 \times 10^{-18}$ cm$^2$.

The molecular oxygen ionization threshold occurs at 1027 Å; however, strong molecular bands continue to be observed to about 600 Å. The photoionization cross section is also shown as it is appreciably different from the total cross section to about 500 Å. The bands may show autoionization structure. Toward the shorter wavelengths of the soft x-ray region, the cross section decreases.

The principal ozone ($O_3$) absorption is centered near 2500 Å. Weaker absorption continues to about 3500 Å toward longer wavelengths. Bands are not shown in the figure.

Molecular nitrogen ($N_2$) begins to absorb strongly at about 1000 Å. Only a few of the numerous bands are shown. A continuum underlying these bands must be weak and an upper limit is shown. The ionization threshold is at 796 Å. A separate photoionization curve is not shown as it is approximately the same as the total absorption curve. Autoionized molecular bands are observed from about 650 to 796 Å.

Atomic oxygen (O) is photoionized at wavelengths shorter than 911 Å. At longer wavelengths absorption is confined to line series converging to the ionization threshold. At wavelengths shorter than 911 Å, there are autoionized series converging to more energetic ionization thresholds. A few of the more intense members are shown.

## 22.3 RATE OF PHOTODISSOCIATION IN THE ATMOSPHERE

Photodissociation resulting in neutral products occurs in the atmosphere due to the absorption of solar radiation by molecules. The photon absorption process resulting in the formation of ions and electrons is called photoionization. It is covered in Chapter 21 of this handbook. In general, photodissociation into neutral products requires less energy than photoionization. It occurs at longer wavelengths and lower altitudes. At many wavelengths and altitudes, both photodissociation into neutral products and photoionization are occurring. The internal and kinetic energy states of the neutral products are very important in determining reaction mechanisms in the atmosphere and where information is available it is included.

This section is an introduction to the most important photodissociation processes and their role in the atmosphere. It is based on Turco and Huffman [1979] and Turco [1975].

The wavelengths of solar radiation of interest in photodissociation are primarily from the strong hydrogen Lyman-alpha line at 1216 Å through the ultraviolet to about 7500 Å. The solar flux available for photodissociation in the ultraviolet at wavelengths less than about 3000 Å is controlled by absorption of molecular oxygen and ozone. This absorption acts as a shutter to decrease the solar flux as a function of altitude and determine the rate of photodissociation of species present at smaller concentrations.

The solar atmospherically attenuated irradiance as a function of solar zenith angle is shown in Figures 22-4, 22-5 and 22-6. Absorption between 3300 and 2000 Å is largely by ozone. Between 2000 Å and 1216 Å, molecular oxygen is the important absorbing molecule. Three representative solar zenith angles of 75°, 60°, and 30° are given in the figures. The oxygen vertical profile is the mean reference profile of Champion [1972]. The ozone profile used is a midlatitude empirical model due to Krueger and Minzer [1976]. The solar flux at the top of the atmosphere used in Figures 22-4, 22-5, and 22-6 is the same as given in Chapter 2 by Heroux and Hinteregger (Figures 2-2, 2-3).

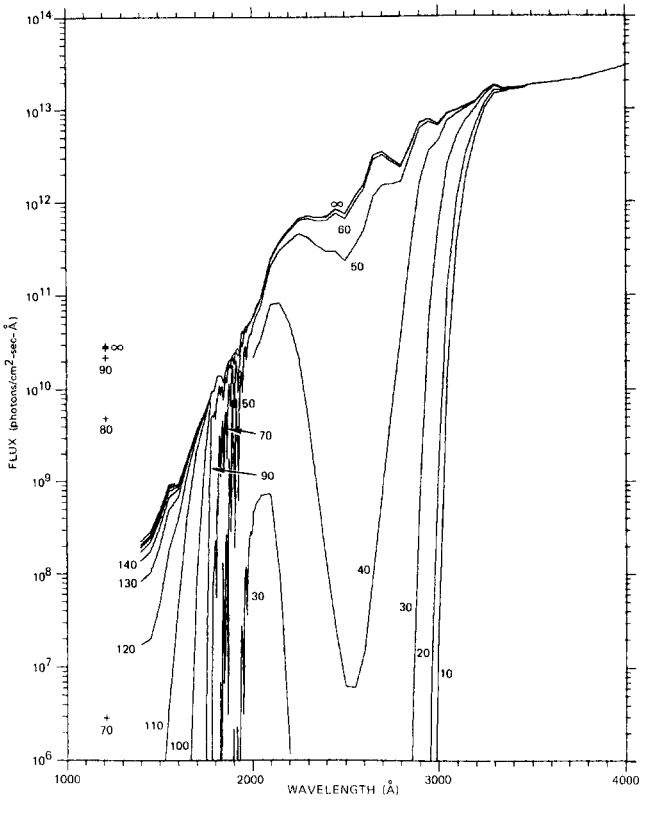


Figure 22-4. Atmospherically attenuated solar irradiance for solar zenith angle of 75° for various altitudes (km).

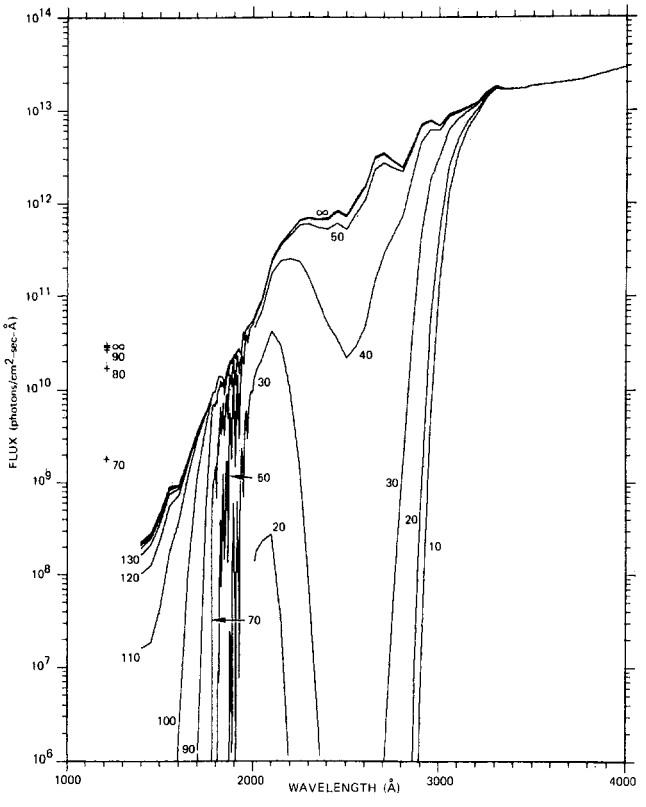


Figure 22-5. Atmospherically attenuated solar irradiance for solar zenith angle of 60° for various altitudes (km).

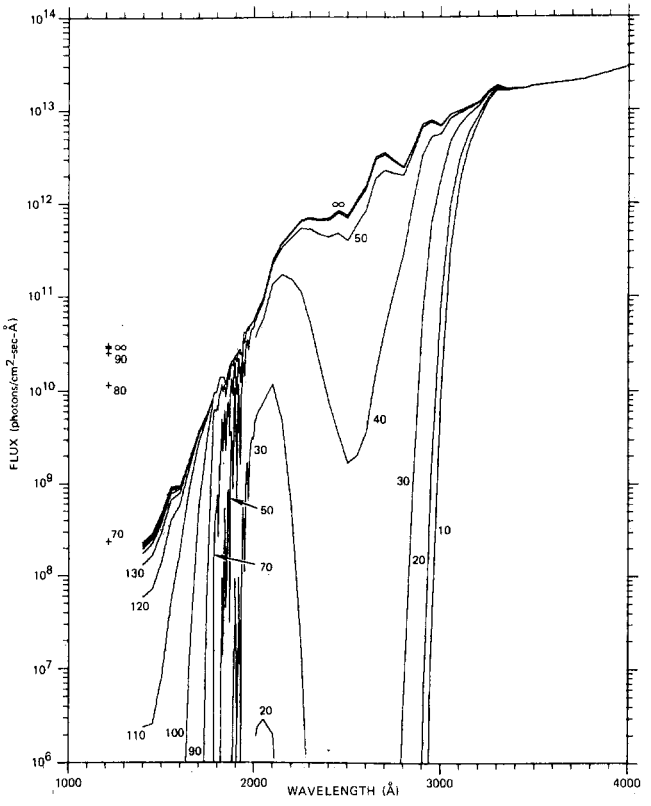


Figure 22-6. Atmospherically attenuated solar irradiance for solar zenith angle of 30° for various altitudes (km).

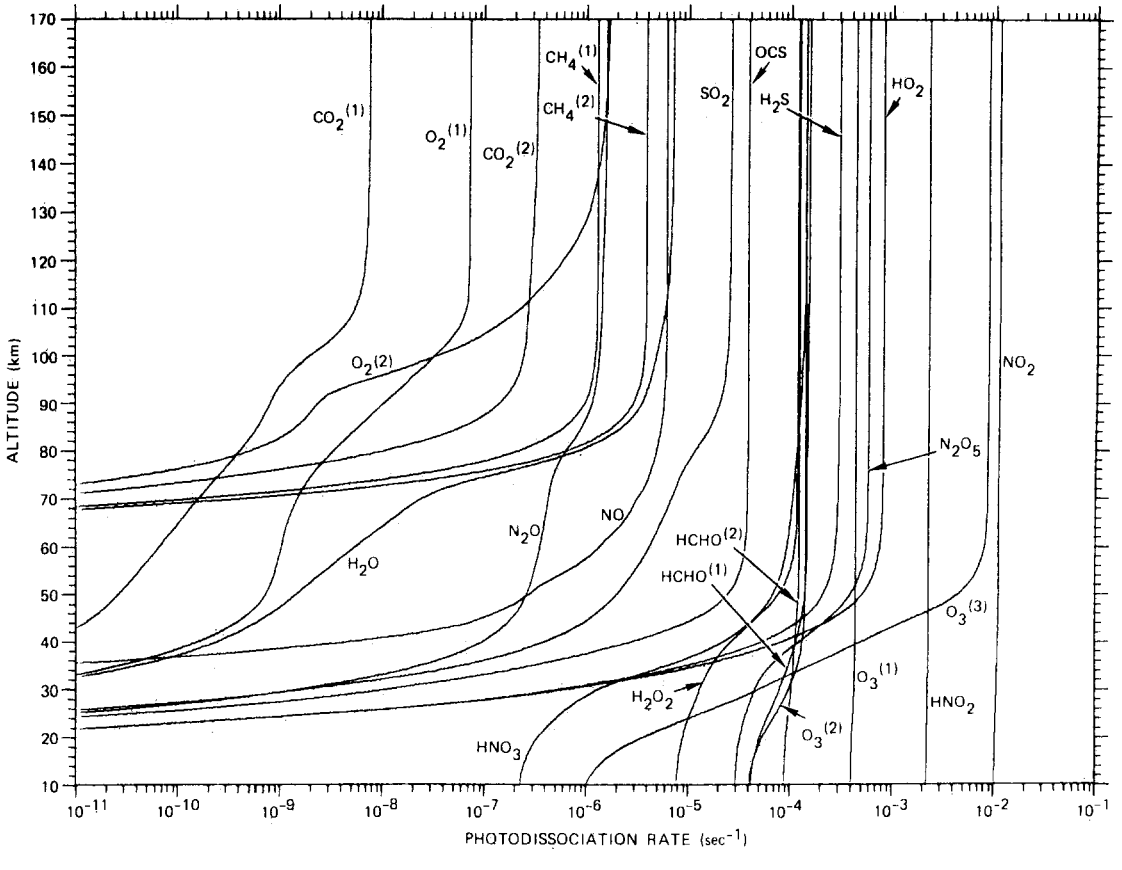


Figure 22-7. Photodissociation rates for solar zenith angle of 75°.

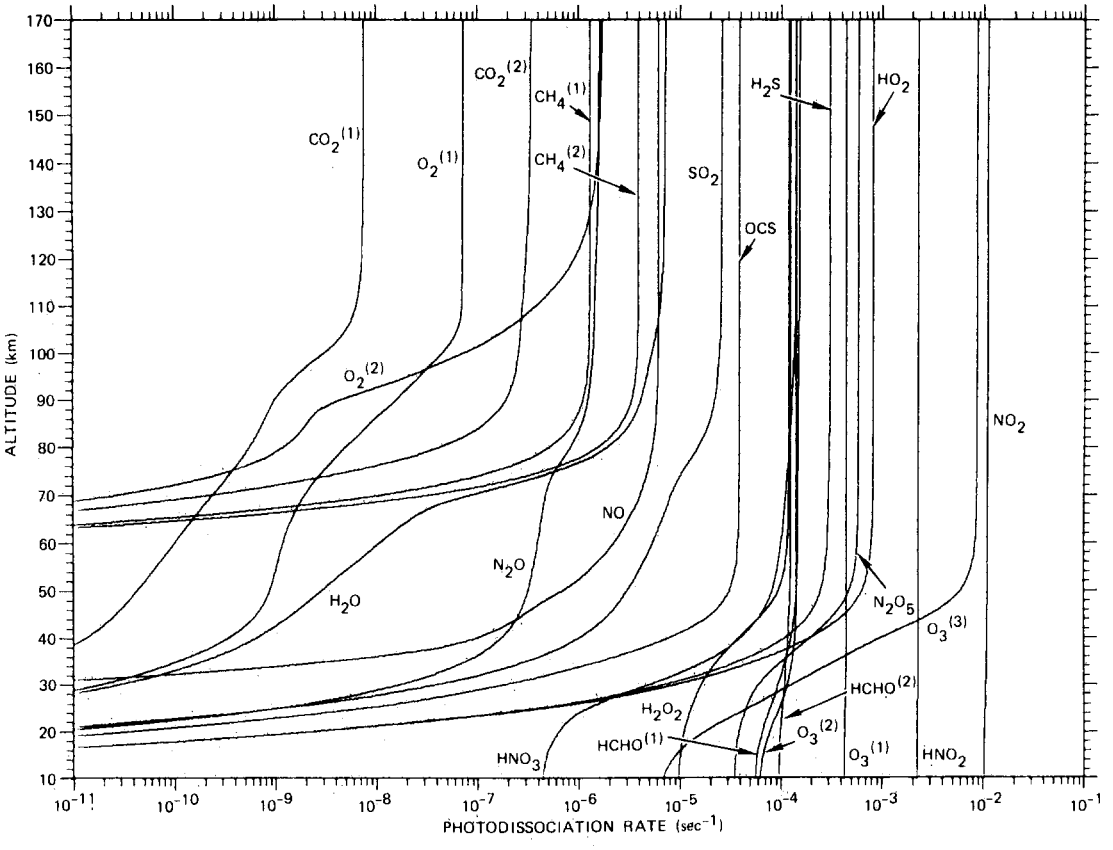


Figure 22-8. Photodissociation rates for solar zenith angle of 60°.

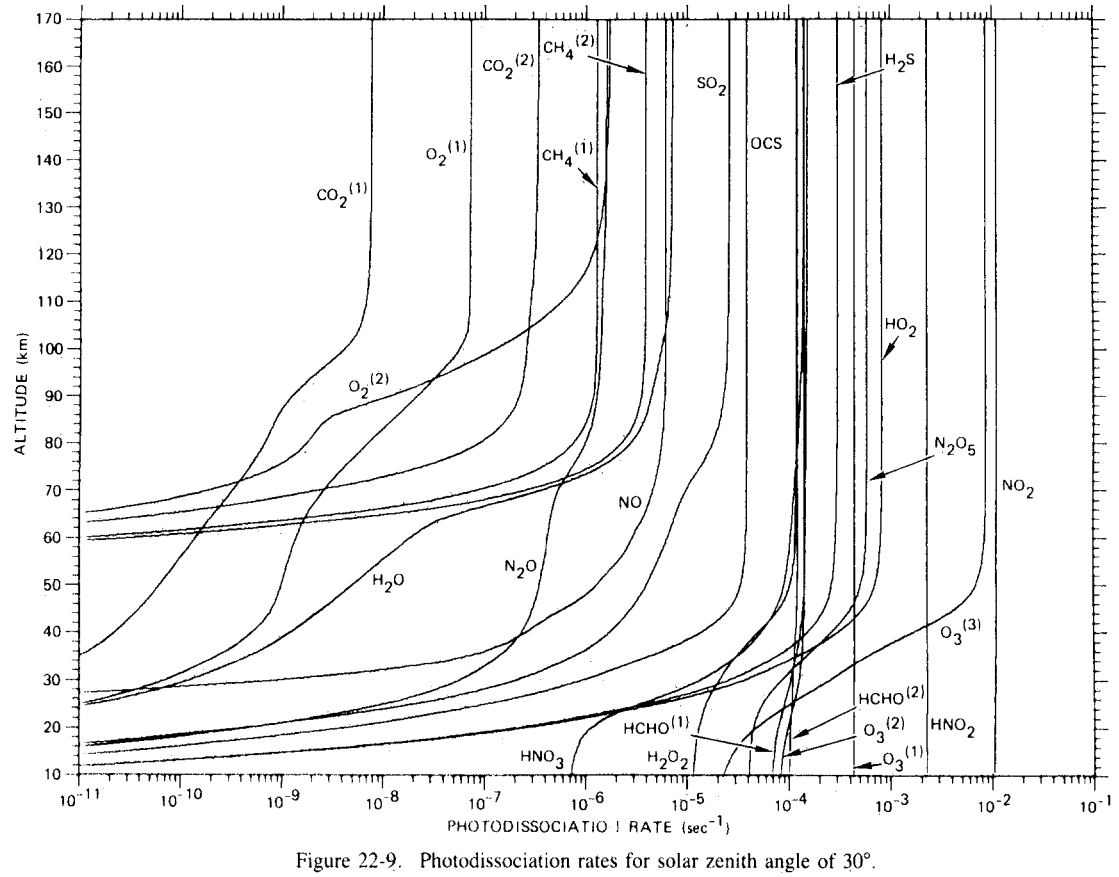


Figure 22-9. Photodissociation rates for solar zenith angle of 30°.

Table 22-2. Molecular photodissociation processes. Product is ground state unless indicated otherwise

| Designation in Figures 22-7, 8 & 9 | Photodissociation Process |
|---|---|
| $O_2(1)$ | $O_2 \rightarrow O + O$ |
| $O_2(2)$ | $O_2 \rightarrow O + O(^1D)$ |
| $O_3(1)$ | $O_3 \rightarrow O + O_2$ |
| $O_3(2)$ | $O_3 \rightarrow O + O_2(^1\Delta_g)$ |
| NO | $NO \rightarrow N + O$ |
| $NO_2$ | $NO_2 \rightarrow NO + O$ |
| $N_2O$ | $N_2O \rightarrow N_2 + O(^1D)$ |
| $N_2O_5$ | $N_2O_5 \rightarrow 2NO_2 + O$ |
| $HNO_2$ | $HNO_2 \rightarrow OH + NO$ |
| $HNO_3$ | $HNO_3 \rightarrow OH + NO_2$ |
| $HO_2$ | $HO_2 \rightarrow OH + O$ |
| $H_2O$ | $H_2O \rightarrow OH + H$ |
| $H_2O_2$ | $H_2O_2 \rightarrow OH + OH$ |
| $CO_2(1)$ | $CO_2 \rightarrow CO + O$ |
| $CO_2(2)$ | $CO_2 \rightarrow CO + O(^1D)$ |
| $CH_4(1)$ | $CH_4 \rightarrow CH_3 + H$ |
| $CH_4(2)$ | $CH_4 \rightarrow CH_2 + H_2$ |
| HCHO(1) | $HCHO \rightarrow CHO + H$ |
| HCHO(2) | $HCHO \rightarrow CO + H_2$ |
| $SO_2$ | $SO_2 \rightarrow SO + O$ |
| OCS | $OCS \rightarrow CO + S(^1D)$ |
| $H_2S$ | $H_2S \rightarrow HS + H$ |

The number of photodissociation events occurring per unit volume per second at a given point in the atmosphere is equal to the local number density multiplied by the photodissociation rate per molecule per second. The latter factor is the integral of the absorption cross section times the solar flux at a given altitude over all significant wavelengths. If known, the cross sections for specific products can also be used to give production rates for specific energy states.

Photodissociation rates are shown in Figures 22-7, 22-8 and 22-9 for the three solar zenith angles of 75°, 60°, and 30°. A total of twenty-three photodissociation processes are shown for seventeen absorbing molecules. The molecules included are $O_2$, $O_3$, NO, $NO_2$, $N_2O$, $N_2O_5$, $HO_2$, $H_2O_2$, $HNO_2$, $HNO_3$, $CO_2$, $CH_4$, HCHO, $SO_2$, $H_2S$, and OCS. The absorption cross sections for $O_2$ and $O_3$ are given in Figure 22-2. References to the remaining cross sections are in Turco and Huffman [1979] and Turco [1975].

The total photodissociation rate per unit volume as a function of altitude can be obtained from Figures 22-7, 22-8, and 22-9 and the number density of the molecule of interest. These densities will vary depending on the problem under consideration. Some of the molecules are included because they are important in the atmospheric chemistry associated with nitrogen oxides, water vapor, and/or other gases released in the atmosphere at greater than naturally occurring levels.

Table 22-2 gives the specific photodissociation reactions that apply to the curves in Figures 22-7, 22-8, and 22-9. In many cases, the excited electronic state of the product is known. The internal energy in the products can be very important in determining subsequent reactions.

## CHAPTER 22

## REFERENCES


Barth, C.A. and E.F. Mackey, "OGO-4 Ultraviolet Airglow Spectrometer," *IEEE Transactions on Geoscience Electronics*, **GE-7** (2): 114–119, 1969.

Barth, C.A. and S. Schaffner, "OGO-4 Spectrometer Measurements of the Tropical Ultraviolet Airglow," *J. Geophys. Res.*, **75:** 4299–4306, 1970.

Barth, C.A., D.W. Rusch, and A.I. Stewart, "The UV Nitric Oxide Experiment for Atmosphere Explorer," *Radio Sci.*, **8:** 379, 1973.

Beiting, E.J. and P.D. Feldman, "A Search for Nitric Oxide Gamma Band Emission in an Aurora," *Geophys. Res. Lett.*, **5:** 51, 1978.

Berkowitz, J., *Photoabsorption, Photoionization and Photoelectron Spectroscopy*, Academic Press, New York, 1979.

Blake, A.J., "An Atmospheric Absorption Model for the Schumann-Runge Bands of Oxygen," *J. Geophys. Res.*, **84:** 3272, 1979.

Carruthers, G.R. and T. Page, "Apollo 16 Far Ultraviolet Imagery of the Polar Auroras, Tropical Airglow Belts, and General Airglow," *J. Geophys. Res.*, **81:** 483–496, 1976a.

Carruthers, G.E., T. Page, and R.R. Meier, "Apollo 16 Lyman-alpha Imagery of the Hydrogen Geocorona," *J. Geophys. Res.*, **81:** 1164–1672, 1976b.

Champion, K.S.W., "The Natural Atmosphere: Atmospheric Structure," *Defense Nuclear Agency Reaction Rate Handbook*, DNA 1948H, edited by M.H. Borner and T. Bauer, Chapter 2, 1972.

Christensen, A.B., "A Rocket Measurement of the Extreme Ultraviolet Dayglow," *Geophys. Res. Lett.*, **3:** 221, 1976.

Chubb, T.A. and G.T. Hicks, "Observations of the Aurora in the Far Ultraviolet from OGO-4," *J. Geophys. Res.*, **75:** 1290–1311, 1970.

Cohen-Sabban, J. and A. Vuillernin, "Ultraviolet Nightglow Spectrum from 1900 Å and 3400 Å," *Astrophys. Space Sci.*, **24:** 127–132, 1973.

Elliot, D.D., M.A. Clark and R.D. Hudson, "Latitude Distribution of the Daytime Ozone Profile above the Peak," Aerospace Report No. TR-0158 (3260-10)-2, 1967.

Feldman, P.D., D.E. Anderson, R.R. Meier, and E.P. Gentieu, "The Ultraviolet Dayglow 4. The Spectrum and Excitation of Singly Ionized Oxygen," *J. Geophys. Res.*, **86:** 3583, 1981.

Gentieu, E.P., P.D. Feldman, and R.R. Meier, "Spectroscopy of the Extreme Ultraviolet Dayglow at 6.5 A Resolution: Atomic and Ionic Emissions Between 530 and 1240 Å," *Geophys. Res. Lett.*, **6:** 325, 1979.

Gerard, J.-C., D.W. Rusch, P.B. Hays, and C.L. Fesen, "The Morphology of Equatorial $Mg^+$ Ion Distribution Deduced from 2800 Å Airglow Observations," *J. Geophys. Res.*, **84:** 5249, 1979.

Heath, D.F., C.L. Mateer, and A.J. Krueger, "The Nimbus-4 Backscatter Ultraviolet (BUV) Atmospheric Ozone Experiment — Two Years Operation," *Pure Appl. Geophys.*, **106–108:** 1238–1253, 1973.

Hicks, G.T. and T.A Chubb, "Equatorial Auroral Airglow in the Far Ultraviolet," *J. Geophys. Res.*, **75:** 6233–6248, 1970.

Hudson, R.D., "Critical Review of Ultraviolet Photoabsorption Cross-Sections for Molecules of Astrophysical and Aeronomic Interest," *Rev. Geophys. Space Phys.*, **9:** 305, 1971.

Huffman, R.E., "Absorption Cross-Sections of Atmospheric Gases for use in Aeronomy," *Canad. J. Chem.*, **47:** 1823, 1969.

Huffman, R.E., F.J. LeBlanc, J.C. Larrabee, and D.E. Paulsen, "Satellite Vacuum Ultraviolet Airglow and Auroral Observations," *J. Geophys. Res.*, **85:** 2201–15, 1980.

Kirby, K., E.R. Constantinides, S. Babeu, M. Oppenheimer, and G.A. Victor, "Photoionization and Photoabsorption Cross Sections of He, O, $N_2$ and $O_2$ for Aeronomic Calculations," *At. Data Nucl. Tables*, **23:** 63, 1979.

Krueger, A.J. and R.A. Minzner, "A Mid-Latitude Ozone Model for the 1976 U.S. Standard Atmosphere," *J. Geophys. Res.*, **81:** 4477, 1976.

Meier, R.R. and P. Mange, "Geocoronal Hydrogen: An Analysis of the Lyman Alpha Airglow Observed from OGO-4," *Planet. Space Sci.*, **18:** 803, 1970.

Meier, R.R. and P. Mange, "Spatial and Temporal Variations of the Lyman Alpha Airglow and Related Atomic Hydrogen Distributions," *Planet. Space Sci.*, **21:** 309–327, 1973.

Meier, R.R., D.J. Strickland, P.D. Feldman, and E.P. Gentieu, "The Ultraviolet Dayglow: I. Far UV Emissions of N and $N_2$," *J. Geophys. Res.*, **85:** 2177, 1980.

Peek, H.M., "Vacuum Ultraviolet Emission from Auroras," *J. Geophys. Res.*, **75:** 6209–6217, 1970.

Prinz, D.K. and R.R. Meier, "OGO-4 Observations of the Lyman-Birge-Hopfield Emission in the Day Airglow," *J. Geophys. Res.*, **76:** 6146–6158, 1971.

Rawcliffe, R.D. and D.D. Eliott, "Latitude Distributions of Ozone at High Altitudes Deduced from Satellite Measurement of the Earth's Radiance at 2840 Å," *J. Geophys. Res.*, **71:** 5077–5089, 1966.

Reed, E.I. and S. Chandra, "The Global Characteristics of Atmospheric Emissions in the Lower Thermosphere and Their Aeronomic Implications," *J. Geophys. Res.*, **80:** 3053–3062, 1975.

Takacs, P.Z. and P.D. Feldman, "Far Ultraviolet Atomic and Molecular Nitrogen Emission in the Dayglow," *J. Geophys. Res.*, **82:** 5011–5023, 1977.

Thomas, G.E., "Lyman-alpha Scattering in the Earth's Hydrogen Geocorona," *J. Geophys. Res.*, **68:** 2639, 1963.

Turco, R.P., "Photodissociation Rates in the Atmosphere Below 100 km," *Geophys. Surveys*, **2:** 153–192, 1975.

Turco, R.P., and R.E Huffman, "Solar Photodissociation in the Atmosphere," *Defense Nuclear Agency Reaction Rate Handbook*, DNA 1948H, edited by M.H. Borner and T. Bauer, Chapter 13B, 1979.

Watanabe, K., "Ultraviolet Absorption Processes in the Upper Atmosphere," *Adv. Geophys.*, **5:** 154, 1958.